JCSE The Journal of Corrosion Science and Engineering

21st Century Corrosion Science

Volume 6 Paper C113

Metal Surfaces with Ultrahydrophobic Properties: Perspectives for Corrosion Protection and Self-Cleaning

M. Thieme[1], R. Frenzel[2], V. Hein[1], H. Worch[1]

[1] Technische Universität Dresden, Institut für Werkstoffwissenschaft, D-01062 Dresden

[2] Institut für Polymerforschung Dresden e.V., Hohe Str. 6, D-01069 Dresden

mithi@rcs.urz.tu-dresden.de

Abstract

This contribution describes the generation of ultrahydrophobic aluminium surfaces in view of improving the corrosion prevention behaviour of this material group. The morphological and chemical prerequisites for ultrahydrophobicity are fulfilled by a treatment which comprises an anodisation step under intensified conditions and a chemical modification. The paper focusses on i) findings gained for the special anodisation procedure and for the produced oxidic layers, such as the composition, micro-structure and micro-hardness, ii) the chemical modification and the wetting properties achieved in dependence on the morphology of the substrates, and iii) results of first tests directed on the evaluation of the resistance of different coating systems towards water and light exposure.

Keywords: aluminium, anodisation, oxide layer, micro-roughness, ultrahydrophobicity, bionics, stability testing

Introduction

Water shows a remarkably ambivalent behaviour with respect to corrosion. On the one hand, it is an essential prerequisite for generating passive layers well-known for iron, nickel, chromium, titanium, aluminium and many other elements and alloys. On the other hand, water molecules play a key role in the course of the active dissolution as the transfer of metal ions from the solid into aqueous electrolyte solutions, which may subsequently be connected with the precipitation of solid, non-protecting layers. One of the traditional ways for preventing metal surfaces from such an attack comprises the formation of separating layers between substrates and media. This strategy is well-known in corrosion science under the designation 'passive corrosion protection'. In the case of aluminium, which exhibits a very high thermodynamic tendency for the formation of its oxide, the surface is usually anodised forming oxidic layers with thicknesses from nanometers up to about 0,1 mm. Normally, this type of conversion layers are very hydro*philic*; porous sub-layers absorb water and with it also dissolved deleterious substances. Moreover, corrosion-stimulating solid particles may deposit on the surface.

On this background, it can be expected that the protecting effect of anodised layers on Al and its alloys will be enhanced, if the separation is combined with water-repelling properties and, even better, with ultrahydrophobic properties, which are connected with self-cleaning effects, too. This property profile is an originally natural strategy, which was evolved in order to minimise deleterious effects of water itself and of micro-biological attack. Clearly, such a strategy has found considerable attention, stimulated by the fundamental investigations of Barthlott and Neinhuis [#ref*01*,*02*] into the water-repelling properties of the leaves of the lotus plant (*Nelumbo nucifera*) and a great number of other herbs. They created the term 'Lotus-effect®' and promoted a bionics-based development in technology. Meanwhile, impacts are recognised in various fields, such as ceramics, plastics and paintings for facades. In each case, certain morphological *and* chemical features must be generated.

We have transferred ultrahydrophobicity to metals such as aluminium and titanium. In contrary to pathways using structured hydrophobic coatings of higher thickness, we produced the required micro-

roughness directly on the metals' surfaces utilising quite different approaches [#ref*03*]. This was followed by a thin-film coating (chemical modification) affecting neither the morphology nor the optical look. Alkyl silanes without or with fluorine-substituted chain, ω-functionalised alkyl silanes, a fluorine-containing co-polymer, and polyelectrolyte/surfactant complexes were successfully employed [#ref*03*], alkanephosphonic acids as well. Efforts are now being made to improve the mechanical stability of the systems developed.

This contribution refers to the major technological pathway elaborated that comprises an anodisation step under intensified conditions, where formation of an oxidic layer and micro-roughening are simultaneously done. The paper focusses on i) findings gained for the special anodisation procedure and for the produced oxidic layers, such as the composition, micro-structure and micro-hardness, ii) the chemical modification and the wetting properties achieved in dependence on the morphology of the substrates, and iii) results of first tests which are directed on the evaluation of the resistance of different coating systems towards water and light exposure.

Experimental

Materials: Pure aluminium EN AW-Al 99.5 (EN AW-1050) was used as well as the materials Al 99.9 (1090; Merck) and Al Mg1 (5005). The size of the sheet specimens was 26x38 mm^2.

Pretreatment: All the specimens were initially undergone a cleaning pre-treatment (abbr. 'P'), consisting of alkaline pickling (1 M NaOH, ambient temperature, 10 min) and neutralising (1 M HNO_3, 60 s);.

Anodisation: For micro-roughening, the specimens were anodised under the following conditions which are designated as 'intensified' (abbr. 'Asi'): stirred solutions of H_2SO_4 and $Al_2(SO_4)_3$ with a total sulphate concentration of 2.3 mol L^{-1} ($c(Al^{3+})_{max}$ = 0.36 mol L^{-1}), temperature T = (40±1) °C, current density j = 28-30 mA cm^{-2}, duration t = 1.2 ks. The specimens were rinsed and water-immersed for at least 3.6 ks.

Other well-known anodisation procedures were applied for comparison [#ref*04,05*]: i) the usual sulphuric acid anodisation (18-20 °C, 15 mA cm^{-2}, 1.5 ks; 'Asu'), ii) conditions for generating greater thickness and hardness of the layer (1.7 M H_2SO_4, 1 °C, 22 mA cm^{-2}, 0.9 ks; 'Ash'), iii) conditions for generating a barrier-type oxide layer (0,5 M $B(OH)_3$ + 0,05 M $Na_2B_4O_7$, ca. 22 °C, 2.5 mA cm^{-2}, max. 40 V; 'Ab'). Additionally, alternative conditions for achieving ultrahydrophobicity (0.5 M H_2SO_4, 10 mA cm^{-2}, 10.8 ks; [#ref*07*]) were tested. Thermal treatments ('T') up to 450 °C were added in some cases.

Mass changes were followed by weighing, where m_1 – starting mass, m_2 – mass after anodisation, m_3 – mass after thermal treatment. These parameters were supplemented by the mass m_4 after stripping the layer in a small volume of 1 M H_2SO_4 and 0.7 M HCl, respectively (40 °C, 2.4 ks). These values were corrected for data obtained with specimens without oxide, because the stripping proved to be not fully selective. Before stripping the specimens were immersed in water for 1 h.

Chemical modification ('cM'): The following solutions were employed:

- hexadecyltrimethoxysilane (HTMS) (5 vol.% in aceton, 3 h),

- tetradecanephosphonic acid (TDPA) (0.1 wt.% in ethanol–water 1+1, 12 h), both for routine testing,
- perfluoroalkyltriethoxysilane (PFATES) (2 vol.% in t-butylmethylether, 3 h),
- [3-(2-aminoethyl)aminopropyl]trimethoxysilane (AAPS) (10 vol.% in ethanol, 3 h) followed by coating with the fluoropolymer poly(tetrafluoroethylene-*co*-2,2'-bis(trifluoromethyl)-4,5-difluoro-1,3-dioxole) (Teflon® AF; DuPont) (0.6 wt.% in perfluoro-(2-perfluoro-n-butyl)-tetrahydrofuran (FC75; 3M)).

Characterisation: The morphology was examined by scanning electron microscopy (Zeiss DSM 982 Gemini) preferably under specimen tilting. Roughness and roughness parameters were assessed by atomic force microscopy (AFM; Digital Instruments Dimension 3100 in tapping mode equipped with Pointprobe or UltraSharp silicon cantilevers; Nanosensors). Additionally, the confocal laser scanning microscopy (Zeiss LSM 510) was used. Metallographic cross-sectioning was done for studying the micro-hardness (Vickers diamond, 50 mN, 20 single measurements on one specimen) and the micro-structure of different oxide types. The latter was accomplished using the etching technique after Weck and *ac* metal deposition from a bath with $SnSO_4$ and $CuSO_4$ [#ref*11*], respectively.

Structural information on the atomic level was derived from X-ray diffraction (XRD; Siemens D 500) and from nuclear magnetic resonance spectrometry (NMR) probing the ^{27}Al nuclei (Bruker MSL 300, magic angle spinning) in the powdered layer material scratched off from the surface.

Water content and binding or adsorption of the modification substances were studied by infrared spectrometry (FT-IRRAS; Perkin-Elmer FTS 2000 equipped with an autoimage microscope and a motorised xyz-stage). Additionally, quantitative analysis of the hydrogen content was accomplished by nuclear reaction analysis (NRA [#ref*08*]) employing the reaction ^{1}H (^{15}N, $\alpha\gamma$) ^{12}C (tandem generator, resonance energy 6.385 MeV, max. dosis ca. 3e+13 ^{15}N, 6 mm^2). Basic information on the composition of the anodic layers was gained from

chemical analyses of the dissolved oxidic layers using complexometry with back titration [#ref*12*] ($m_{Al,ox}$ – mass of Al in the layer), ICP-MS (Perkin-Elmer ELAN 5000; $m_{Al,ox}$*, $m_{Mg,ox}$*) and ion chromatography (Metrohm, equipped with suppressor and conductivity detector; $m_{SO4,ox}$). The stripping had been optimised before in view of selectivity and completeness. Small acid volumes of 1 M H_2SO_4 and 0.7 M HCl, respectively, were used (40 °C, 2400 s; m_4 – mass after stripping).

The wetting properties were characterised by dynamic contact angle (DCA) measurements (Krüss DSA10) based on 3-5 sites on each specimen.

Stability tests: i) Water spraying using a home-made setup, which directed a fine water beam (ca. 1 ml s^{-1}) in an angle of 45° onto the centre of the specimens. An area of about 40 mm^2 was affected. Durations of 4 h, 24 h and 100 h were employed including specimens with HTMS, PFATES and Teflon® AF coatings.

ii) Constant-climate tests according to DIN 50017-KK (40 °C, 100 wt.% relative moisture under dewing, exposure 360 h) including TDPA, PFATES and Teflon® AF coatings, 8 specimens each.

iii) Simulating weathering tests according to DIN EN ISO 11341, Zyklus A, comprising a change of moistening and drying (period length 2 h) combined with Xenon lamp radiation (exposure 360 h; Institut für Korrosionsschutz Dresden GmbH). Likewise, TDPA-, PFATES- and Teflon® AF-coated specimens (4 of each) were tested.

Results and Discussion

Characteristics of the intensified anodisation process

Electrochemical features: Chronopotentiometric curves of the anodic process are characterised by an initially steep potential rise up to a maximum at about 12 V, which is reached after a few seconds pointing to the fast buildup of the barrier film (see below). In the following a potential plateau is formed at a level of 9-10 V. The slight variation of the potential heights reflect the different conductivity of the solutions according to the varying H^+-to-Al^{3+} ratio. The curves are similar to those for the usual anodisation conditions where the potential levels

are higher by about 2 V. This indicates that the oxide forming proceeds qualitatively in a similar manner.

Mass analysis: Further insight into the anodisation process was gained from the analysis of the mass parameters in dependence on the anodisation time t (Fig. 1a). The value $(m_2-m_1)/A$, which is connected with the anodisation process itself, passes a shallow maximum for anodisation times of about 0.3 ks and moves into the negative range beyond 0.6 ks, i.e. the specimens are undergone an increasing mass loss in the course of anodisation. The specific oxide mass $(m_2-m_4)/A$ grows up to a limiting value of about 2.5 mg cm^{-2} for anodisation times of more than 1.2 ks, disregarding the potential constancy from about 10 s on. The overall metal loss described by $(m_4-m_1)/A$ obeys Faraday's law very correctly. This means that the transformation of Al into Al(III) proceeds exclusively on electrochemical basis.

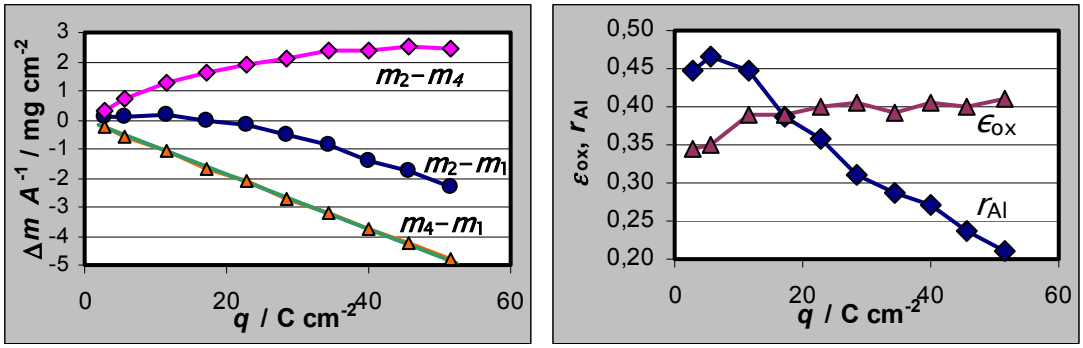

Fig. 1. Characteristics of the anodisation under intensified T, j conditions and medium stirring intensity for varied anodic charge density q; a) specific mass changes $\Delta m/A$ and spec. metal loss acc. to Faraday's law (green line); b) oxide formation effectivity ϵ_{ox} acc. to (1) based on m_4-m_1, and mass ratio r_{Al} acc. to (2); means of 2–8 single data.

Oxide formation effectivity: The degree of the formation of the oxidic layer was characterised by the oxide formation effectivity ϵ_{ox} as that portion of the oxidised Al(III) which is bound in the layer ($m_{Al,ox}$ as determined by complexometric titration following the selective dissolution) ratioed by the total metal loss. The latter quantity may be substituted by the charge density q as stated above:

$$\varepsilon_{ox} = \frac{m_{Al,ox}}{m_4 - m_1} = \frac{zF}{M_{Al}} \frac{m_{Al,ox} / A}{q} \quad (1)$$

Fig. 1b shows the course of ϵ_{ox} vs. q. The oxide formation effectivity has a maximum of $\epsilon_{ox} \approx 0.45$ at the beginning of the anodisation (possibly with the exception of the first point at 100 s), whereon it decreases with increasing duration in a practically linear manner down to about 0.2. Interestingly, experiments *without* stirring resulted in even lower effectivities ($\Delta\epsilon_{ox} = -(0.1–0.15)$ for $t = 800–1200$ s). Similar results were obtained with Al 99.9 and Al Mg1. It should be noted that the relatively low values of the effectivity may be disadvantageous from an economic point of view, but this is a consequence of the occurring reactions which are leading to the specific morphology (see below) as the major target of the anodic treatment.

It is well-known that the oxide formation effectivity of the usual anodisation process is much higher due to the lower temperature. Comparative measurements gave values of nearly 80 wt.%.

Morphology and wetting properties

After anodisation under the intensified conditions according to the ‘Asi’ procedure stated, the surface is given a micro-roughness characterised by non-regularly ordered mountain-like structure elements of typically 1–2 µm in distance and height (Fig. 2a, b). Additionally, a very fine, sub-µm-scale roughness can be seen. Contrarily, the usual anodisation ‘Asu’ is characterised by a more or less flat, shell-like shaped (oxidic) surface (Fig. 2c). Subsequent hot-water sealing may lead to a complete change of the respective morphologies.

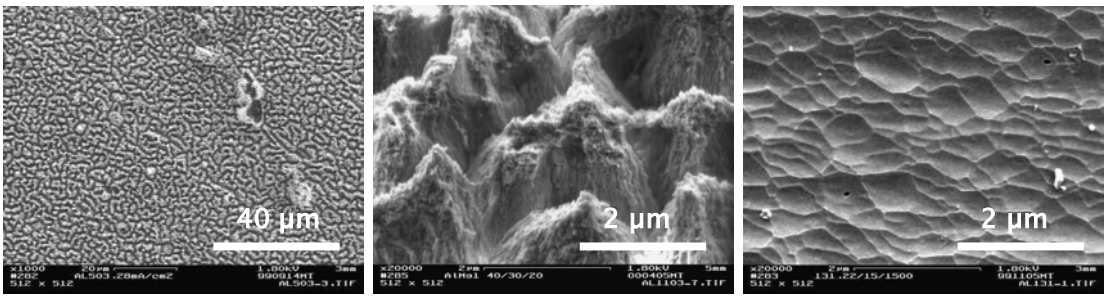

Fig. 2. SEM images of differently anodised surfaces; a) Al 99.5, ‘P’ + ‘Asi’; b) Al Mg1, ‘P’ + ‘Asi’ (35° tilted); c) Al 99.5, ‘P’ + ‘Asu’.

These features have been proved to be decisive in view of the issue, whether or not the surface will display ultrahydrophobicity. Only on micro-rough surfaces, advancing and receding angles of 150–160° each were received, following an appropriate chemical modification treatment (see below).

Whereas the 'Asi'-produced surface was very uniform on Al 99.9, with Al 99.5 hole-like features (dimension of about 10 µm, Fig. 2a) occurred additionally. These regions are ascribed to oxygen gas evolution at sites of impurities in the material [#ref*06*]. The wetting properties were not affected.

Surprisingly, the treatment conditions given by Shibuichi and co-workers [#ref*07*] did not produce a suitable roughness and, hence, failed in achieving ultrahydrophobicity.

In view of generating micro-rough surfaces and ultrahydrophobic properties, a closer examination of the influence of the anodisation parameters led to the following conclusions:

- The anodisation time had to exceed a certain minimum duration to produce the micro-rough surface type. At $T = 40$ °C, $j = 28$ mA cm^{-2} a minimum duration of about 1.0 ks was found; however, influences of the temperature and the stirring rate were detected (Fig. 3). A sharp change in the microscopic shape may occur in between only 0.1 ks during anodisation.

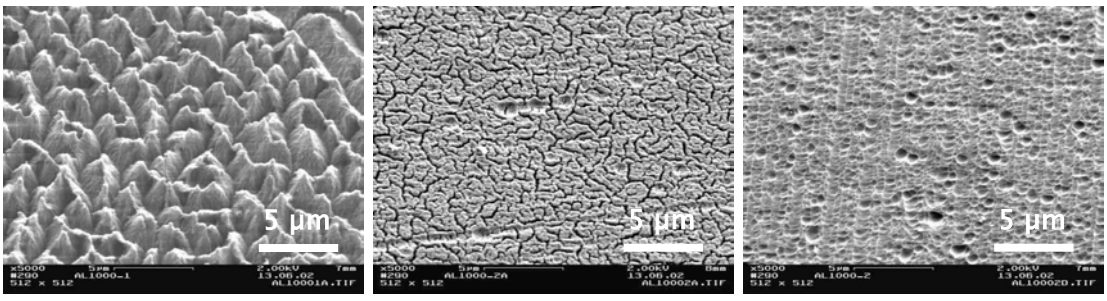

Fig. 3. SEM images (35° tilted) of anodised surfaces under increasing stirring intensity (a–c); Al 99.9, 'P' + 'Asi', $t = 1.0$ ks.

- The temperature showed a 'treatment window' which ranges altogether from 35 °C to 50 °C at $j = 28$ mA cm^{-2}, $t = 1.5$ ks. This window becomes more narrow for $t = 1.2$ ks.

At 40 °C, the current density could be varied from 28 up to 42 mA cm^{-2} (or even more) without changing the microscopic shape and, hence, the wetting behaviour. Disadvantageous effects of a lower c.d. could not be compensated for by prolonged duration, i.e. the charge density is an important, but not the decisive quantity.

Structural and mechanical properties

No characteristic features of any oxyhydroxide or hydroxide compounds could be gained by X-ray diffraction measurements on anodised specimens, independent of the anodisation type.

NMR revealed that the Al atoms are surrounded by O in a non-uniform manner. AlO_4, AlO_5 and AlO_6 coordination was found at the same time, thus excluding the presence of a certain crystalline compound. Rather an amorphous structure should be present. The same holds for the powder material after a thermal treatment at 450 °C, 3.6 ks. XRD detected traces of bayerite γ-$Al(OH)_3$.

Infrared measurements pointed to a difference between 'Asi'- and 'Asu'-generated layers comparing the region below 900 cm^{-1}, in which the Al-O binding is displayed (Fig. 4). This reflects a different atomic binding for Al, even after tempering (see below).

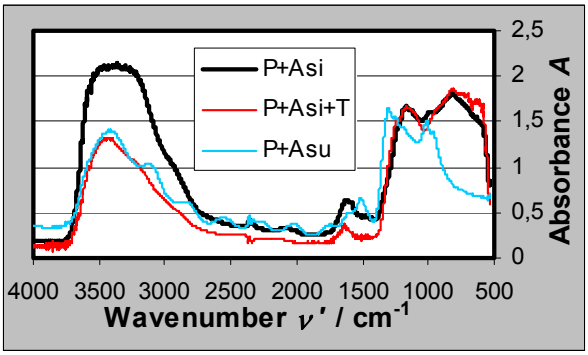

Fig. 4. FT-IRRAS results of specimens after different anodisation (plus thermal treatment).

Images of cross-sections indicated an average layer thickness of about 10 µm with a profile height of 2 µm. Stripping of the oxidic layer led to a specific mass loss of 2.3 mg cm^{-2} corresponding to a density of about 2.3 g cm^{-3}, which is similar to the tabulated value of 2.42 g cm^{-3}

for $Al(OH)_3$, but considerably lower than for Al_2O_3 (3.90 g cm^{-3} [#ref *13*,*14*]).

Under high magnification, SEM images of cross-sections revealed the porous, anisotropic nature of the major part of the layer. This finding could be unambiguously visualised by 'decorating' the pores with a highly contrasting metal filling (Fig. 5a). Additionally, the cross-sections were etched to achieve a greater differentiation of the bulk of the layer. Fig. 5b demonstrates that the outer part of the layer underneath the micro-rough surface appears uniform, whereas the inner part shows a fibre-like micro-structure, which means that the chemical stability of the oxidic substance is locally different. This statement was true also for 'Asu'-type oxides (Fig. 5c).

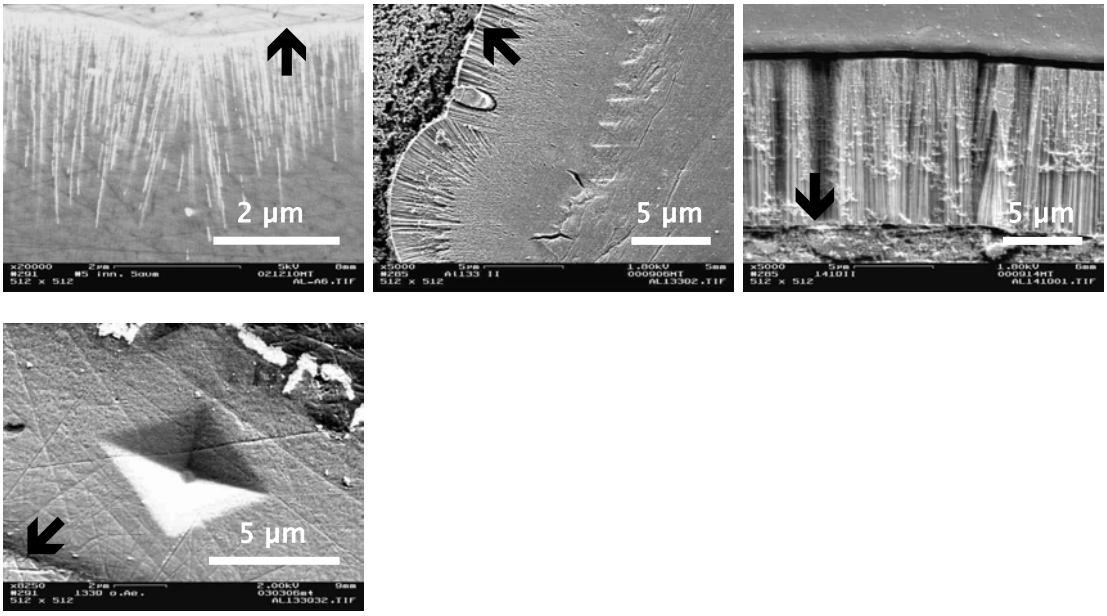

Fig. 5. SEM images of cross-sections; a) 'P' + 'Asi' plus cathodic deposition of Sn/Cu into the pore grounds of the oxidic layer; b) 'P' + 'Asi', cross-section etched; c) 'P' + 'Asu', cross-section etched; d) 'P' + 'Asi' + Cu evaporated for contrasting, micro-hardness indent in the oxidic layer; substrate-layer interfaces marked by arrows.

Micro-hardness indents were nearly regularly shaped without any cracks (Fig. 5d). This points to a certain degree of compressibility, which is obviously larger in the lateral direction, as is expressed by the marked asymmetry of the indents. The micro-hardness amounted to

250–290 HV 0.005 / 5 for 'Asi'-produced layers on Al and Al Mg1. This was probably somewhat lower than for 'Asu' (296±34 for T = 23 °C, 343±33 for 16 °C). The standard deviation on a single specimen was in the range ±10–15 %. Of course, the hardness of 'Ash'-type specimens was highest (403±30). Thermal post-treatments may lead to an enhancement of the micro-hardness, especially with Al Mg1.

Interestingly, the subsequent application of coating systems (see below) influences the micro-hardness of the oxidic layer. Whereas an enhancing tendency was found for specimens treated in non-aqueous media containing silanes, the micro-hardness was considerably diminished by employing TDPA solution, which contain water in a high concentration (e.g. 253 HV 0.005 → 168 HV 0.005 for an Al Mg1 specimen). However, TDPA solution did *not* reduce the mechanical stability following a thermal treatment. Thus, re-hydratisation phenomena can be limited or even prevented.

Analytical results referring to the oxidic layers

Al content: The content of Al in the oxidic layer was ratioed by its total mass in order to get a first information on what compound the layer substance might represent:

$$r_{\mathrm{Al}} = \frac{m_{\mathrm{Al,ox}}}{m_2 - m_4} \qquad (2)$$

For instance, AlOOH (= $Al_2O_3 \cdot H_2O$) would correspond to a mass ratio r_{Al} = 0.45, $Al(OH)_3$ (=$Al_2O_3 \cdot 3H_2O$) to r_{Al} = 0,35. The experimental results (Fig. 1b) gave values of r_{Al} = 0.34–0.41 with an increasing tendency in the course of anodisation. This means the composition would lie between the hydroxide and the oxyhydroxide, if an oxidic compound without further components was preliminarily assumed.

Mg content: The analysis data based on ICP-MS gave practically the same Mg/Al mass ratio as in the original material.

Water content: The anodic layers contain a noticeable content of water depending on the type of anodisation, but also on the degree of the preceding water immersion. The content of hydroxyl groups and/or incorporated water molecules could be semi-quantitatively determined

by FT-IRRAS investigation based on the region of 3400–3500 cm^{-1}. The ‘Asi’ layers contained markedly more water than ‘Asu’ layers (Fig. 4). Moreover, the measurements showed that the water concentration in ‘Asi’-type layers was reduced by thermal treatment down to the level of ‘Asu’ layers. However, a complete de-hydratisation could not be achieved under the conditions chosen (400 °C, 0.9–3.6 ks). This finding does not correspond to the statements given for the thermal transformation of bayerite and hydrargillite [#ref*13*].

Based on gravimetrical control, the amount of the desorbed water reached a limit of 3–4 wt.% in the temperature range of 350–450 °C. However, this content is not a constant. Following a prolonged water immersion of 20 h, a much greater water amount was indicated by IRRAS and the thermally removed portion was higher (10 wt.%).

These results were contrasted by data from NRA referring to a depth of about 1 µm. Here, two parts could be discriminated: i) easily removable hydrogen, probably owing to physically adsorbed water, ii) stationary concentrations. The total concentrations were calculated as atomic ratios to $r_{H,at}$ = 18.8 at.% H (‘Asi’) and 7.4 at.% H (‘Asu’). Assuming again a hydroxidic-oxidic compound of the formula $Al_2O_3 \cdot xH_2O$ for the ‘Asi’-produced layer type, the following values may be assessed for x: $x_{therm} \approx 0.22$ and $x_{NRA} \approx 0.65$, respectively. The discrepancy $x_{therm} \neq x_{NRA}$ underlines that a great portion of the total amount of incorporated water appears to be bound relatively strongly.

Sulphate incorporation: Sulphate was qualitatively indicated by IRRAS (S–O binding, 950–1000 cm^{-1}). Based on mass data, a mass ratio analogous to (2) was defined. Values of $r_{SO4} \approx 0.17$ were found, equal to data for usual anodic layers formed in sulphuric acid media [#ref*05*]. This means that the simplified formula $Al_2O_3 \cdot xH_2O$ of the layer substance should no longer be acceptable.

Formation and composition of the oxidic layer

From all these findings ideas about the formation of the layer may be derived. The principal composition of the layer type generated by intensified anodisation is similar to the usually acid-produced oxide [#ref*05*]. Thereafter, the composite layer consists of a very thin barrier

film at the metal–oxide interface and a much thicker sub-layer of porous nature (Fig. 5a, b). The total potential decay is divided between the resistance of the solid state conduction process in the barrier film (thickness $d_b \approx 0.9$ nm [#ref*05*]) and, to a presumably lesser extent, the electrolyte resistance in the pores. The layer growth takes place primarily at the interfaces of the barrier film connected with the transport of Al^{3+} and O^{2-} ions through the defective oxidic solid according to the brutto reaction

$$2\ Al + (3+x)\ H_2O \rightarrow Al_2O_3{\cdot}(H_2O)_x + 6\ H^+ + 6\ e^- \qquad (3)$$

At the same time, a transformation of the barrier layer into the porous layer proceeds so that d_b remains constant. Obviously, the interior structure of the porous sub-layer is formed under the influence of the electric field (Fig. 5a, b). In the pores and at the outer interface, equilibria of the form

$$Al^{3+} + x\ H_2O \leftrightarrow Al(OH)_x^{(3-x)+} + x\ H^+ \qquad (4)$$

will establish regulating dissolution and precipitation.

Additionally, the ions SO_4^{2-} and HSO_4^- from the electrolyte solution will participate in the reactions and incorporate into the solid. Substituting now $Al_2O_3{\cdot}xH_2O$ by the extended formula $Al_2[O_{3-y-z/2}\,(SO_4^{2-})_y\,(HSO_4^-)_z]{\cdot}xH_2O$ and assuming $y << z$ because of the dissociation equilibria of H_2SO_4, it is possible to give a rough idea about the composition of the layer substance. From the experimental mass ratio data ($r_{Al} \approx 0.40$, $r_{SO4} \approx 0.17$ and $r_{H,at} \approx 0.19$) and the corresponding molar masses the coefficients $z \approx 0.24$ and $x \approx 0.52$ are calculated for layers produced under ‘Asi’ conditions.

The thickness growth of the porous layer is increasingly limited by the chemical dissolution at the outer interface, until a stationary state will establish. The stirring effect may be understood considering the heat production at the ground and in the pores of the layer. In case of an unstirred solution the temperature rise will inevitably lead to a more intensive dissolution, connected with stronger profiling (Fig. 3a) and a decrease of the oxide forming effectivity compared to stirring.

Chemical modification and wetting properties

Extensive selection tests were carried out for choosing suitable hydrophobic compounds. This led to the employment of various compound groups, such as differently functionalised reactive alkylsilanes, alkanephosphonic acids, fluoropolymers, and polyelectrolyte/surfactant complexes, which can covalently react with the hydroxylated surface, simply adsorbed or electrostatically bound [#ref*03*].

For routine preparation, the application of an easy silane was sought. Fig. 6 displays a comparison of the wetting behaviour based on 'P'-treated (non-anodised) Al 99.9 and coatings of alkyltrialkoxysilanes, which are expected to react with the solid (**s**) primarily according to:

$$\mathbf{s}\text{–OH} + (\text{R–O})_3\text{SiC}_n\text{H}_{2n+1} \rightarrow \mathbf{s}\text{–O–Si(OR)}_2\text{C}_n\text{H}_{2n+1} + \text{R–O–H} \qquad (5)$$

The wetting angles, especially θ_r, increased with increasing chain length up to n ≈ 16. Therefore, HTMS was chosen as a standard compound.

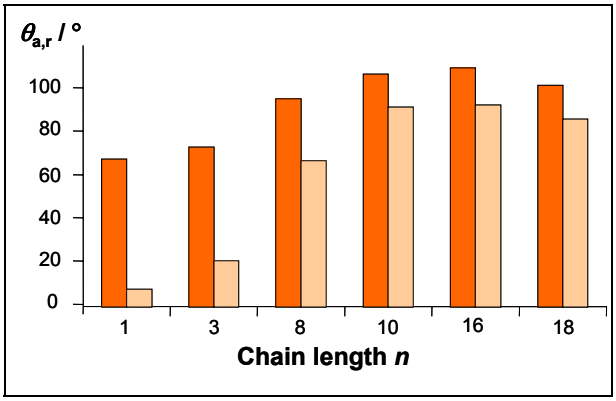

Fig. 6. Wetting angles θ_a (left bars) and θ_r (right bars) of 'P'-treated Al 99.9 following a modification using alkyltrialkoxysilanes $(C_nH_{2n+1}Si(OR)_3$.

Wetting angle data for different pretreatments and HTMS modification are compiled in Table 1. For the 'Asi'-treated surface type, ultrahydrophobicity was clearly achieved. The corresponding contact angle hysteresis ($\theta_a - \theta_r$) was mostly negligible. Water droplets will roll off the specimen even in case of a minute inclination. The most striking differences to the non-roughened surface types are seen for

the receding angles. As expected, all the non-coated surface types were completely wettable in a fresh state.

Treatment	θ_a / °	θ_r / °
'P' + 'Asi' (sulphuric acid, *T*, *j* intensified, *t* = 1.2–1.5 ks) + 'cM' (HTMS)	151–161	144–160
'P' + 'cM' (HTMS)	108	70
'P' + 'Ab' (borate buffer) + 'cM' (HTMS)	113–128	29–86
'P' + 'Asu' (sulphuric acid, *T*, *j* regular) + 'cM' (HTMS)	80–105	26–62
'P' + 'As' (*j* intensified) + 'cM' (HTMS)	79±3	21±4
'P' + 'As' (*T* intensified) + 'cM' (HTMS)	145±1	103±13
'P' + 'As' [#ref↗] + 'cM' (HTMS)	110±0.3	22±5

Table 1. Comparison of wetting properties of differently treated surface types (data scattering: standard deviation for one specimen, span widths for several specimens).

Altogether, ultrahydrophobicity was achieved employing HTMS, chlorosilanes, PFATES, TDPA, Teflon and others based on micro-roughened oxidic surfaces, thus forming inorganic–organic hybrid systems. The modification coatings can generally not be detected by means of SEM. IRRAS investigations, however, indicated typical features of the coatings additionally to those owing to the substrates (Fig. 7): i) alkyl chains of HTMS and TDPA (C–H stretch, 2800–3000 cm^{-1}), ii) C–F binding preferably of the alkyl chains with PFATES (1250 cm^{-1}).

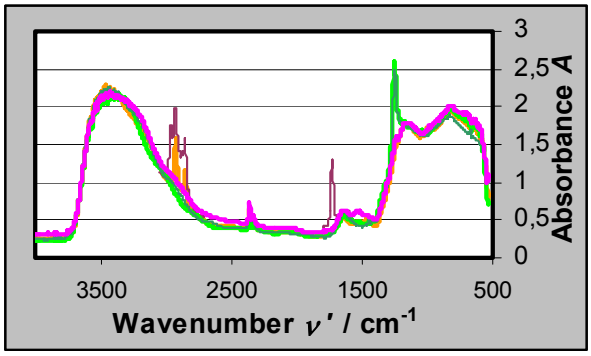

Fig. 7. FT-IRRAS results of coated specimens following 'P'+'Asi'; orange – HTMS, light green – PFATES, pink – AAPS / Teflon® AF; brown (single bands) – HTMS after water spray test, dark green – PFATES after water spray test.

The quantitative determination of surface energies is only restrictedly possible, because this quantity is not defined for a material-air composite surface, as is in fact produced by the intensified anodisation (cf. below). The maximum wetting angle values measured for more or less flat surfaces plus modification correspond to surface energies of $\gamma_{s,min}$ = 6-8 mJ m^{-2} based on the equation of Li and Neumann [#ref*09*]:

$$\cos\theta_a = -1 + 2\sqrt{\frac{\gamma_s}{\gamma_l}}\exp(-\beta(\gamma_l - \gamma_s)^2) \qquad (6)$$

where γ_l – surface tension of water as the test liquid (72.8 mJ m^{-2}) and β – constant (β = 0.0001247 m^2 mJ^{-1}). It should be noted that this level of the surface energy is equal to the value given for the trifluoromethyl group (ca. 6 mJ m^{-2}), whereas it is considerably lower than for flat PTFE (18.5 mJ m^{-2} [#ref*07*])

For micro-profiled and chemically modified substrates, the profile-bearing area t_p to a resting water droplet may be assessed according to the formula given by Cassie and Baxter [#ref*10*]:

$$\cos\theta_{rough} = t_p \cdot \cos\theta_{smooth} - (1 - t_p) \qquad (7)$$

A level of only 10 wt.% is obtained for ultrahydrophobic surfaces. The corresponding force for the droplet to start rolling on such a surface is

estimated to be in the sub-μN region, what explains the behaviour mentioned above.

Stability evaluation

Water spray test: These tests comprised HTMS, PFATES and AAPS / Teflon® AF as coatings based on a 'P' + 'Asi' treatment. In the beginning, the fine water beam bounced back vividly from all specimens involved. This was expected from the wetting angle data. With HTMS, the contact area enlarged after 2 h only. After 100 h a dramatic deterioration was observed (θ_a = 120-125° and θ_r < 10°). Whereas the IR spectrum showed no change after 4 h, the examination of the wetted area after 100 h revealed some alterations, the most prominent of which was a new band at 1730 cm^{-1} that must be ascribed to the formation of a C=O group (Fig. 7). The AAPS / Teflon® AF coating showed a noticeably better behaviour, although at termination of the test the bouncing effect had disappeared and the DCA values were reduced (140°/10°). Most stability could be stated with the PFATES-coated specimens. Here, the visual wetting behaviour had only slightly changed connected with moderately reduced receding angles (158°/159° → 142-153°/130°). The IR spectra were practically identical with the original state (Fig. 7).

Constant-climate test: The tests over 360 h were passed without noticeable deterioration of the wetting properties for PFATES and Teflon® AF coatings. TDPA-modified surfaces retained ultrahydrophobicity, but showed a decrease of the wetting angles by a few degrees (2-5°).

Simulating weathering test: The wetting data received before and after this test are displayed in Fig. 8. According to the degree of the wetting angles' decrease the resistance towards dewing/drying and light radiation is ranking according to: TDPA << AAPS / Teflon® AF < PFATES.

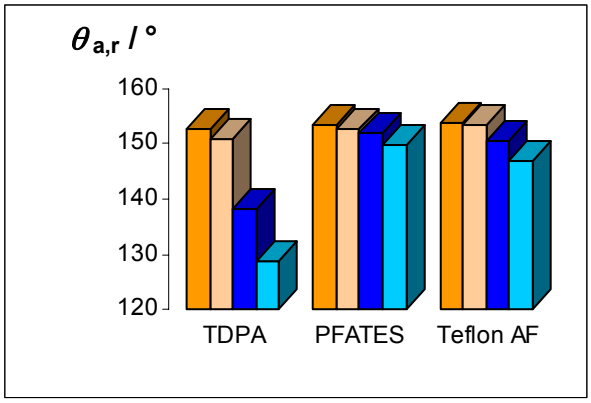

Fig. 8. Comparison of the wetting data (θ_a/ θ_r) for differently coated specimen types; yellowish bars – original state, bluish bars – after the simulating weathering test.

Conclusions

Ultrahydrophobic aluminium surfaces were successfully generated based on an intensified anodisation process, which aims at forming a micro-roughened oxidic surface, and a subsequent chemical modification using various hydrophobic compounds. Characteristic data were determined for the specific oxide mass and the oxide formation effectivity, which is remarkably lower than with the usually employed anodisation. Information was gained on structural properties and the composition, which is characterised by a markedly higher portion of water. In first tests under water and light exposure, the silane coating type with a fluorinated alkyl chain shows the highest stability among the coating compounds investigated. This may be a promising finding in view of further developments and testing. Although the micro-hardness of the oxidic layers is fairly high, the total hybrid system is relatively sensitive to scratching. This issue is under investigation at present.

Acknowledgments: The authors are indebted to valuable experimental contributions of R. Born, M. Ruhnow, T. Fuhrmann, U. Cikalo, R. Süptitz (Technische Universität Dresden), A. Hennig (Institut für Polymerforschung Dresden e.V.), E. Brendler (Technische Universität Bergakademie Freiberg), U. Schaefer, D. Birnstein, D. Grambole

(Forschungszentrum Rossendorf e.V.). The financial support by the Sächsisches Staatsministerium für Wissenschaft und Kunst (contract no. 4-7533-70-821-98/3) and the Bundesministerium für Bildung und Forschung (FKZ 03C0340B) is gratefully acknowledged.

References

!ref*01* 'Purity of the sacred lotus, or escape from contamination in biological surfaces', W. Barthlott, C. Neinhuis, *Planta*, **202**, pp1-8, 1997.

!ref*02* 'Characterization and distribution of water-repellent, self-cleaning plant surfaces', C. Neinhuis, W. Barthlott, *Annals of Botany*, **79**, pp667-677, 1997.

!ref*03* 'Generation of ultrahydrophobic properties of aluminium – a first step to self-cleaning transparently coated metal surfaces', M. Thieme, R. Frenzel, S. Schmidt, F. Simon, A. Hennig, H. Worch, K. Lunkwitz, D. Scharnweber, *Adv. Engin. Mater.*, **3**, 9, pp691-695, 2001.

!ref*04* ' Characterization of thin barrier oxide layers on aluminum alloys using electrochemical impedance spectroscopy', C. A. Gervasi, J. R. Vilche, in: *Proc. Symp. 'Oxide Films on Metals and Alloys'*, Proc. Vol. **92-22**, Pennington, NJ: The Electrochem. Soc., pp139-147, 1992.

!ref*05* 'Oberflächenbehandlung von Aluminium', T. W. Jelinek, Saulgau: Leuze, 1997.

!ref*06* 'Residual flaws due to formation of oxygen bubbles in anodic alumina', A. C. Crossland et al., *Corros. Sci.*, **41**, pp1945-1954, 1999.

!ref*07* 'Superölabstoßende Oberflächen', K. Tsujii et al., *Angew. Chem.*, **109**, pp1042-1044, 1997; 'Super water- and oil-repellent surfaces resulting from fractal structure', S. Shibuichi et al., *J. Colloid Interf. Sci.*, **208**, pp287-294, 1998.

!ref*08*, http://www.fz-rossendorf.de/pls/robis/info?id=307&lang=de.

!ref*09*, 'Contact angles on hydrophobic solid surfaces and their interpretation', D. Li, A. W. Neumann, *J. Colloid Interf. Sci.* **148**, pp190-200, 1992.

!ref*10*, in : 'Ultrahydrophobic polymer surfaces prepared by simultaneous ablation of polypropylene and sputtering of poly(tetrafluoroethylene) using radio frequency plasma', J. P. Youngblood, T. J. McCarthy, *Macromolecules* **32**, pp6800-6806, 1999.

!ref*11*, http://www.chemie.uni-oldenburg.de/didaktik/peter3.htm.

!ref*12*, 'Maßanalyse', G. Jander, K. F. Jahr, Berlin, New York: de Gruyter, 1989.

!ref*13*, 'Lehrbuch der Anorganischen Chemie', H. Remy, Leipzig: Geest & Portig, p424, 1965.

!ref*14*, 'Tabellenbuch Chemie', R. Kaltofen et al., Thun, Frankfurt am Main: Deutsch, 1998.